Letter

Anomalous Hall effect in thin bismuth

Oulin Yu,[1] Sujatha Vijayakrishnan,[1] R. Allgayer,[2] T. Szkopek,[3] and G. Gervais[1]
[1]*Department of Physics, McGill University, Montreal, Québec, Canada H3A 2T8*
[2]*Department of Mining and Materials Engineering, McGill University, Montreal, Québec, Canada H3A 2B1*
[3]*Department of Electrical and Computer Engineering, McGill University, Montreal, Québec, Canada H3A 0E9*

(Received 1 December 2023; accepted 28 February 2024; published 18 March 2024)

Bismuth, the heaviest of all stable group V elements with strong spin-orbit coupling, is famously known to exhibit many interesting transport properties, and effects such as Shubnikov-de Haas and de Haas-van Alphen were first revealed in its bulk form. However, the transport properties have not yet been fully explored experimentally in thin bismuth nor in its two-dimensional limit. In this work, bismuth flakes with average thicknesses ranging from 29 to 69 nm were mechanically exfoliated by a microtrench technique and were used to fabricate four-point devices. Due to the mixing of components, Onsager's relations were used to extract the longitudinal (R_{xx}) and Hall (R_{xy}) resistances where the latter shows a Hall anomaly that is consistent with the anomalous Hall effect. Our work strongly suggests that that there could be a hidden mechanism for time-reversal symmetry breaking in pure bismuth thin films.

DOI: 10.1103/PhysRevB.109.L121406

Introduction. The anomalous Hall effect (AHE) was discovered by Edwin Hall only a year after his discovery of the ordinary Hall effect. However, unlike the classical Hall effect that was immediately rationalized, the mechanism for the AHE remained the subject of debate for nearly a century. Today, it is believed that the AHE has two types of contributions [1,2]: an *intrinsic*, scattering-free mechanism originally proposed by Karplus and Luttinger [3] that can also be reconciled with the presence of a Berry curvature [see Fig. 1(a)], as well as scattering-dependent mechanisms known as *extrinsic* contributions [see Fig. 1(b)]. Despite these advances in the 1950s, the AHE remains poorly understood in certain systems such as, for example, spin glasses. Notably with the recent emergence of topologically nontrivial band structures, the study and understanding of the AHE in these materials led to a renaissance of interest in the topic.

Bismuth is the heaviest stable group V element ($Z = 83$) and has, therefore, a very large spin-orbit coupling (SOC) [4,5]. However, due to inversion symmetry in the bulk Bi crystal, the bulk itinerant carriers do not experience SOC, in contrast to the surface-state carriers. Bismuth in the bulk form has been extensively studied and has a long history of exhibiting celebrated transport properties. Remarkably, effects such as the Shubnikov–de Haas (SdH) effect, the de Haas–van Alphen effect, and the Nernst-Ettingshausen effect were first discovered in bismuth. Recently, in part due to the discovery of graphene, interest in bismuth has been revived for its predicted properties in thin layered structures and in its two-dimensional form known as bismuthene. For instance, a semimetal to semiconductor transition is predicted to occur when its thickness reaches 30 nm or less [6–8], but finding such a transition has been proven to be experimentally difficult due to fabrication challenges and the potentially nontrivial contribution of surface states [4]. Yet, quantum confinement is important in understanding transport properties of films of thickness up to about 100 nm [9–11]. Furthermore, advances were made in isolating the single-layer allotrope, bismuthene, and it was successfully grown for the first time on a SiC substrate in 2017 [12], albeit its transport properties still await to be unraveled experimentally. More recently, there has been a widespread interest in bismuth as there is substantial evidence for it to be a higher-order topological insulator [13,14] and to host intrinsic superconductivity where the transition occurs below $T_c \approx 0.5$ mK [15]. As such, this makes bismuth an excellent candidate in which to study the AHE in a system that is topologically nontrivial.

If time-reversal symmetry (TRS) is broken in bismuth, then one would expect it to manifest the intrinsic AHE [1,2]. For instance, the work of Hirai *et al.* on 30-nm bismuth film experimentally demonstrated that circularly polarized light can open a gap in the bismuth's band structure, leading to time-reversal symmetry breaking which then leads to an AHE [16]. Moreover, in a model proposed by Haldane in 1988, he argues that TRS breaking on a honeycomb lattice can lead to a quantum anomalous Hall effect (QAHE) [17]. The QAHE was observed by Chang *et al.* [18] in 2013, and in 2018 Young *et al.* [19] experimentally found the QAHE in twisted bilayer graphene where TRS was broken when the interlayer twist angle in the moiré pattern is $\theta \approx 1.1^\circ$. Here, we report on our work in sub-100-nm bismuth films whereby an unambiguous signature of the AHE was observed in electronic transport measurements. Bismuth is known to be a diamagnetic material and as such the manifestation of the AHE requires the breaking of TRS which is, to our knowledge, unexpected. Our observation of the AHE in pure bismuth suggests that a hidden mechanism must be responsible for the TRS breaking. This discovery is not only important to further understand the already extensively studied properties of bismuth but also to extend our comprehension of the AHE.

Method. We developed a technique using the microtrench structure to mechanically exfoliate thin bismuth flakes [20]. The microtrench structure was prepared by etching a SiO_2

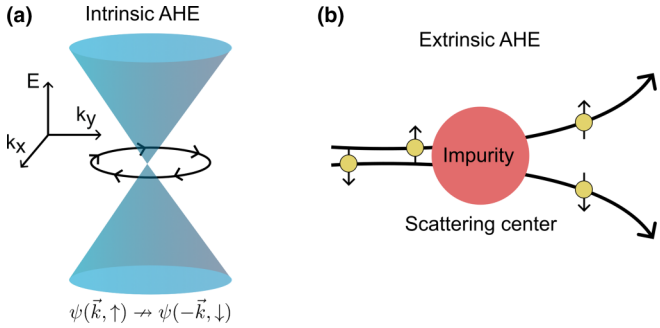

FIG. 1. (a) The intrinsic AHE arises from time-reversal symmetry (TRS) breaking intrinsic to the electronic structure. (b) The extrinsic AHE arises from impurity scattering mechanisms that break the TRS.

thermal oxide layer above a degenerately doped silicon substrate, effectively turning it to a mechanical file. As shown in Fig. 2(a), a bulk bismuth crystal, with its orientation carefully chosen to be the (1,1,1) surface, was attached to the tip of a metal pen. By grating the bismuth crystal against the microtrench file, thin flakes of bismuth were obtained and found to be as thin as ∼10 nm [20]. Such mechanical exfoliation provides a way to obtain ultrathin bismuth flakes in a clean and controlled environment. In particular, compared to the recently reported exfoliation methods using liquid sonication [21,22], water and oxygen that are detrimental to electronic properties can be avoided. While molecular beam epitaxy (MBE) techniques can produce films down to 3 nm [23], our method is far more straightforward to prepare high-quality flakes down to comparable thicknesses.

Thin bismuth flakes with average thicknesses of 29 to 69 nm were obtained and characterized by atomic force microscopy (AFM) (see Supplemental Information [24]). Note that the flakes have height variations, and only the average height is quoted here. Ti/Au contacts were deposited via electron beam lithography (EBL) and electron beam vapor deposition. Note that the environment was carefully controlled with all fabrication steps performed in a vacuum or in a nitrogen-filled glovebox. Lastly, a polymethyl methacrylate capping layer was spin-coated for protecting the bismuth flake against oxidization. An optical image of a 68-nm device fabricated in the van der Pauw (vdP) geometry is shown in Fig. 2(c), with the schematic shown in Fig. 2(b). Two other devices fabricated in a comb geometry are shown in the Supplemental Material [24]. Note that due to the small size of the flake (∼1 × 1 μm), as we discuss below, the ohmic contacts are subject to misalignments and hence mixing of electronic transport components is to be expected.

The chemical nature of bismuth flakes was confirmed via Raman spectroscopy with a Bruker Senterra confocal Raman equipped with a 785-nm laser. The flake was compared to its bulk counterpart of the same crystal as a benchmark. The small Raman signal of the flake is due to its small size; however, it is still possible to observe the 70- and 97-cm^{-1} Raman shift peaks associated with pure bismuth [25,26] [see Fig. 2(e), red]. Additionally, the most common type of bismuth oxide typically formed at lower temperatures ($\lesssim$300 °C), β-Bi_2O_3, was observed in the bulk crystal (blue) at 125 and 313 cm^{-1} [27–29] but not in the exfoliated flake.

The temperature dependence of the resistance of the van der Pauw device is plotted in Fig. 2(d) from 3 to 250 K and is consistent with previously reported values for bulk semimetallic bismuth [30,31] as well as thin films down to 500 nm [32].

Results and Discussion. The small size and the limitation imposed by EBL resulted in the van der Pauw contacts to be deposited relatively close to each other, as can be seen in Fig. 2(c). Since the contacts are not exactly at the corners as depicted in Fig. 2(b), the longitudinal (XX) and Hall (XY) resistances are expected to be mixed to some degree in every

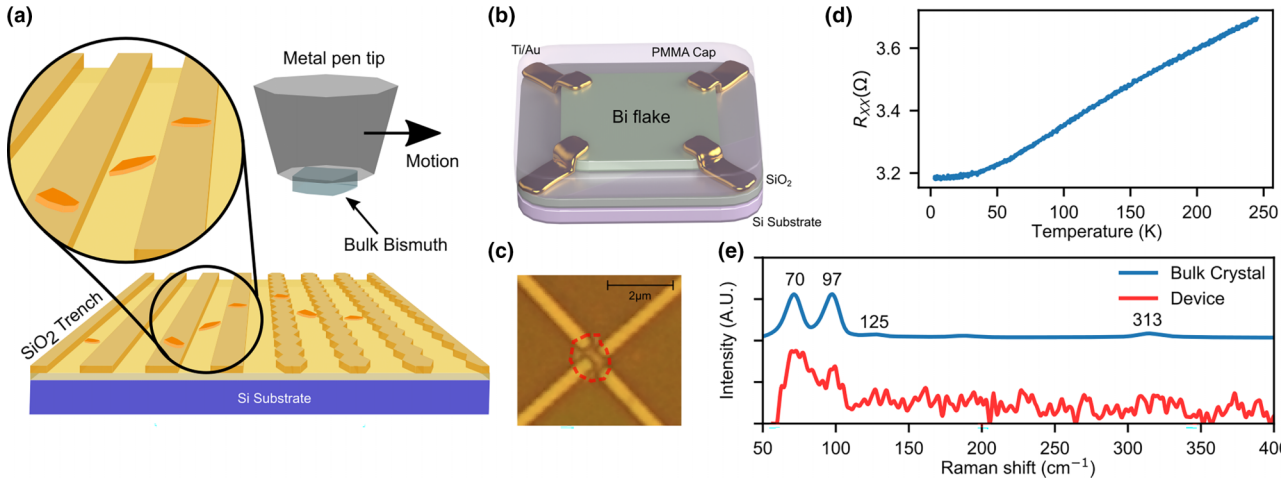

FIG. 2. (a) Mechanical exfoliation of bismuth by grating a bulk bismuth crystal against SiO_2 micro-trench structures. (b) Schematic of the device and (c) optical microscope image of the fabricated device in the van der Pauw configuration where the red dashed lines indicate the perimeter of the flake as confirmed by AFM (see Supplemental Material [24]). (d) Four-point resistance as a function of temperature. (e) Raman spectroscopy of the device compared to its bulk counterpart. Note that 70 and 97 cm^{-1} are Stokes shifts for pure bismuth, whereas bismuth oxide β-Bi_2O_3 has a Raman peak at 313 cm^{-1} which was not observed for the device. Raman spectra were normalized to the bismuth peak of 70 cm^{-1}.

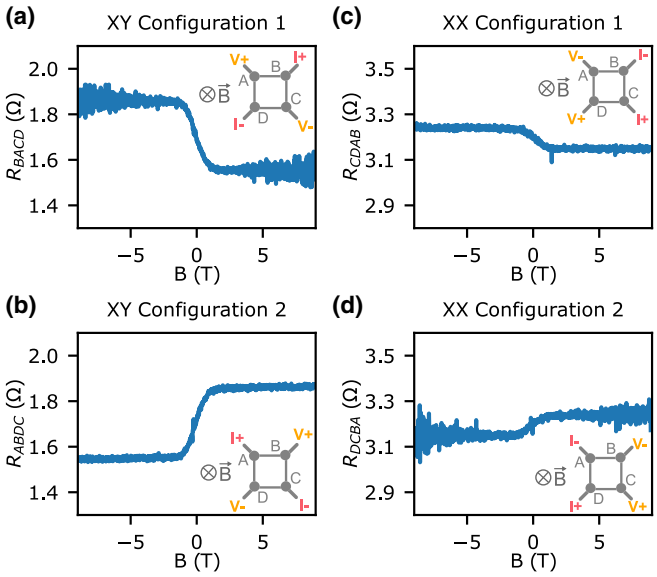

FIG. 3. Four-point resistances of different probing configurations versus magnetic field B (positive defined as pointed into the page) at 15 mK. Panels (a) and (b) are in the XY configurations and form an Onsager pair, and panels (c) and (d) are in the XX configurations and are also Onsager reciprocals. The contact configurations are shown in the insets.

probe configuration. To overcome this mixing, we use the Onsager symmetrization to reconstruct the true longitudinal R_{xx} and Hall R_{xy} resistances. According to Onsager's reciprocity theorem [33], inverting the current and voltage contacts in a linear system allows us to measure the transpose of the resistance tensor given by

$$R(B) = \begin{pmatrix} R_{xx} & R_{xy} \\ -R_{xy} & R_{xx} \end{pmatrix},$$

where B is the applied magnetic field. Consequently, by measuring the resistance in one configuration as well as its Onsager reciprocal, the true longitudinal R_{xx} and Hall R_{xy} resistances can be obtained by respectively symmetrizing and antisymmetrizing the two configurations with

$$R_{xx} = \frac{R + R'}{2}$$

and

$$R_{xy} = \frac{R - R'}{2},$$

where R and R' form an Onsager pair. For example, a four-point measurement configuration labeled ABCD (corresponding to probes I+/V+/V−/I−) would have its Onsager reciprocal with the contact configuration BADC.

The resistances versus magnetic fields (with the positive field defined as pointed into the page, see Fig. 3 insets) were measured at 15 mK and are shown in Fig. 3. We stress that mixing of the R_{xx} and R_{xy} was inevitably observed; however, Figs. 3(a) and 3(b) are XY configurations that maximize the Hall signal and that are also Onsager reciprocals to one another. Similarly, Figs. 3(c) and 3(d) are the XX configurations

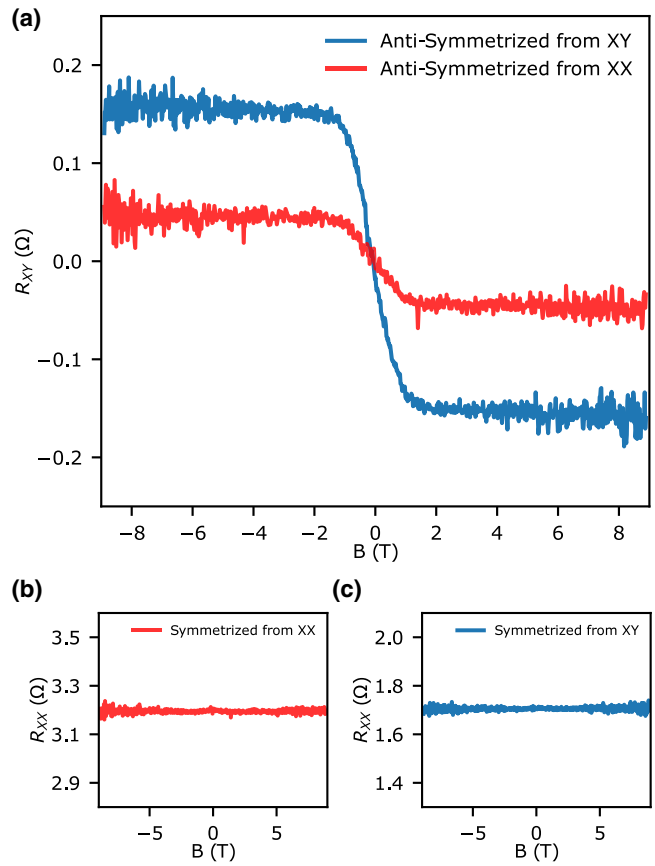

FIG. 4. (a) R_{xy} extracted from XX and XY Onsager pairs through antisymmetrization, showing the Hall anomaly. Panels (b) and (c) are the extracted R_{xx} from the same Onsager pairs.

that optimize the XX signal while also capturing a mixed Hall signal. The corresponding ideal probe configurations in the van der Pauw geometry are shown in the insets of Fig. 3.

Figure 4 summarizes our main result: the extracted true Hall and longitudinal resistances as a function of the magnetic field B. Figure 4(a) shows the antisymmetrized signal from the XY configurations, and as expected it is greater than the antisymmetrized signal from the XX configurations. Similarly, the true longitudinal signal symmetrized in a similar fashion is shown in Figs. 4(b) and 4(c) for the XX and XY configuration pairs, respectively. In particular, both true R_{xx} are constant as a function of the magnetic field up to ± 9 T. The resistance values are 3.2 Ω (extracted from XX) and 1.7 Ω (extracted from XY). The difference in the extracted resistances is attributed to the contacts that are not equidistant from one another, as the ratio of the R_{xx} resistances is approximately equal to the ratio of the distances between the voltage probes.

From the Hall response shown in Fig. 4(a), careful inspection of the data shows the presence of a very small slope in the saturated regime of the Hall signal. In particular, for the XY configuration's saturated high-field region ($|B| \geqslant 2$ T), a fit to the linear slope yields the value $-0.0010(4)$ Ω/T, and similarly a linear fit to the XY configuration's low-field region ($|B| \leqslant 0.5$ T) yields a slope of $-0.174(3)$ Ω/T (see the Supplemental Material [24] for the detailed extraction of these values). While the negative values found for both linear Hall

signals support the electronic transport being hole-dominated, it is unfortunately not possible to reliably extract carrier densities and mobilities because the constancy of the R_{xx} shown in Figs. 4(a) and 4(b) is uncharacteristic of the multicarrier model. Bismuth is known to host both electron and hole pockets in the bulk [34,35], as well as in thin films [36–38]. If both carriers were present, R_{xx} could only saturate at high fields if the densities of electrons and holes were unequal, i.e., $n \neq p$. The characteristic field for this saturation is given by [39]

$$B^{\star} = \frac{n\mu_p + p\mu_n}{|n-p|\mu_n\mu_p},$$

where n and p are electron and hole densities, and μ_n and μ_p are electron and hole mobilities. Note that the reduced Hall slope observed at high fields in Fig. 4(a) implies that $|n - p| \ll 1$, which leads to a very high saturation field for R_{xx}. Under such saturation, R_{xx} would have a magnetic field dependence $\propto B^2$, and if R_{xy} were dominated by a low-density, high-mobility carrier at low fields, it would have a magnetic field dependence $\propto B^3$. Neither of these are observed in our work. Carrier density in bismuth can also have a field-dependent effect [39–41], but the linearity of R_{xy} with B at high field implies that density variation is not responsible for the observations made here. Moreover, the elongated Fermi surface pockets known for bulk bismuth [4] can strongly affect the transport behavior. That being said, the multicarrier model discussed above is valid as long as the Fermi surfaces are closed. Meanwhile, the possibility of an open orbit in the Fermi surface can be excluded because it is inconsistent with the saturation of R_{xx} at high field as observed in our experiments. All things considered, we cannot reconcile the multicarrier model with the Hall and magnetotransport data presented in this work. Furthermore, in contrast to bulk bismuth where quantum oscillations can be observed well under 1 T [42], in our case we did not observe any SdH oscillations in the longitudinal resistance. As we discuss below, this unexpected behavior was nevertheless observed previously in a 100-nm-thick film grown by MBE [32].

Using the device geometry and the longitudinal resistance measured in the absence of a magnetic field, the conductivity is calculated to be $\sigma_{xx} \sim 10^5$ $(\Omega\text{cm})^{-1}$ which places the bismuth device in a good-metal regime dominated by scattering-independent mechanisms [1]. It is indeed expected for bismuth to manifest the intrinsic AHE [1,2] because of its high SOC. However, TRS breaking is a necessary condition for both intrinsic and extrinsic AHEs, and as such, SOC alone is not sufficient to explain the AHE signal observed here. Usually, intrinsic TRS breaking is achieved by ferro- or antiferromagnetism, but bulk bismuth is known to be the most diamagnetic element with a magnetic susceptibility value of -1.66×10^{-4} [43]. Consequently, unless a magnetic transition would occur as the thickness of bismuth is reduced, TRS breaking must originate from elsewhere. Interestingly, in their growth and characterization of bismuth thin films by MBE, Partin *et al.* found a Hall resistivity and magnetoresistivity nearly identical to our data for their thinnest 100-nm bismuth film (see Fig. 6 of Ref. [32]). Specifically, their magnetoresistivity in the 100-nm film was found to be independent of the magnetic field and the Hall resistivity shows a similar AHE behavior with a saturation near 1 T, as is observed in our work. Importantly, the work of Partin *et al.* [32] found more conventional behavior for films thicker than 100 nm, leading to the observation of SdH oscillations which are absent in the 100-nm film even for magnetic fields as high as 17 T. The complete featureless and flat trend observed in their and our works for bismuth of similar thicknesses remains an intriguing mystery.

More recently, Camargo *et al.* claimed to have observed the AHE in bulk bismuth but were unable to find the source of the TRS breaking either [44]. A portion of their work was dedicated to eliminating magnetic contamination and superconductivity, and it was concluded that the AHE may arise from the topologically nontrivial surface or hinge states rather than in the bulk. Such arguments align with our observation of the AHE in thin devices with average flake thicknesses of 68 (main text), 29, and 69 nm (see Supplemental Material [24]). Strikingly, these two other devices were fabricated in a comb geometry, yet the four-probe resistances demonstrated a magnetic field response similar to that of AHE measured in the vdP device presented in the main section of our Letter. While the longitudinal resistances of the vdP and comb devices were different (2 to 32 Ω), the anomalous Hall responses were unexpectedly similar (0.1 to 0.4 Ω), hinting that the observed AHE does not arise from the bulk, but instead from the surface. The resistance's temperature dependence, which is consistent with that of the bulk bismuth down to 500 nm, also supports this observation as it suggests that the bulk is measured simultaneously with the surface or hinge states.

Finally, in addition to a nontrivial topology in bismuth [12–14,45], there are also other prospect origins for spontaneous TRS breaking. These include band flattening as in the case of twisted bilayer graphene, orbital magnetism of Dirac electrons that could arise in bismuth, and strain-induced band distortion [46–48], all of which could lead to a broken TRS. There is a long sequence of works supporting an intrinsic AHE in bismuth. From Conn and Donovan's work in the late 1940s which found traces of AHE [44,49,50] to the recent work by Camargo *et al.* for the bulk [44], as well as our own work in exfoliated bismuth that is consistent with Partin *et al.*'s [32] MBE-grown 100-nm bismuth thin film, all these works point towards a *bona fide* intrinsic AHE occurring in bismuth with an unknown origin of broken TRS.

Conclusion. We successfully fabricated sub-100-nm bismuth devices and studied their electronic transport properties. Bismuth's measured Hall resistance is consistent with the anomalous Hall effect despite bismuth being highly diamagnetic. Our results strongly suggest that there must exist a mechanism for breaking TRS in bismuth which needs to be further investigated and understood. In future works, we expect to explore the Hall anomaly at higher magnetic fields and at different field-effect gate voltages to obtain a better understanding of its electronic band structure as well as a more profound comprehension of its predicted nontrivial topology. As such, and in spite of having been one of the most extensively studied materials since the 19th century, bismuth remains a fascinating elemental material that has yet to be fully understood.

Acknowledgments. This work has been supported by the Natural Sciences and Engineering Research Council of Canada, Canadian Institute for Advanced Research, the Canadian Foundation for Innovation, and the Fonds de Recherche du Québec Nature et Technologies. Sample fabrication was carried out at the McGill Nanotools Microfabrication facility and GCM Lab at Polytechnique Montréal. We would like to thank R. Talbot, R. Gagnon, and J. Smeros for technical assistance, M.-H. Bernier for helpful electron-beam lithography discussions, I. Garate for useful discussions of the theory, and finally Y. Wang for three-dimensional drawings of the device. R. Allgayer acknowledges financial support from a Vanier Canada Graduate Scholarship.

[1] N. Nagaosa, J. Sinova, S. Onoda, A. H. MacDonald, and N. P. Ong, Anomalous Hall effect, Rev. Mod. Phys. **82**, 1539 (2010).

[2] D. Culcer, in *Encyclopedia of Condensed Matter Physics (Second Edition)*, edited by T. Chakraborty (Academic Press, 2024), Vol. 1, p. 587.

[3] R. Karplus and J. M. Luttinger, Hall effect in ferromagnetics, Phys. Rev. **95**, 1154 (1954).

[4] Ph. Hofmann, The surfaces of bismuth: Structural and electronic properties, Prog. Surf. Sci. **81**, 191 (2006).

[5] X. Gonze, J.-P. Michenaud, and J.-P. Vigneron, *Ab initio* calculations of bismuth properties, including spin-orbit coupling, Phys. Scr. **37**, 785 (1988).

[6] V. B. Sandomirskiĭ, Quantum size effect in a semimetal film, J. Exp. Theor. Phys. **25**, 101 (1967).

[7] C. A. Hoffman, J. R. Meyer, F. J. Bartoli, A. Di Venere, X. J. Yi, C. L. Hou, H. C. Wang, J. B. Ketterson, and G. K. Wong, Semimetal-to-semiconductor transition in bismuth thin films, Phys. Rev. B **48**, 11431 (1993).

[8] T. Hirahara, T. Shirai, T. Hajiri, M. Matsunami, K. Tanaka, S. Kimura, S. Hasegawa, and K. Kobayashi, Role of quantum and surface-state effects in the bulk Fermi-level position of ultrathin Bi films, Phys. Rev. Lett. **115**, 106803 (2015).

[9] S. Xiao, D. Wei, and X. Jin, Bi(111) thin film with insulating interior but metallic surfaces, Phys. Rev. Lett. **109**, 166805 (2012).

[10] N. Marcano, S. Sangiao, C. Magén, L. Morellón, M. R. Ibarra, M. Plaza, L. Pérez, and J. M. De Teresa, Role of the surface states in the magnetotransport properties of ultrathin bismuth films, Phys. Rev. B **82**, 125326 (2010).

[11] Z. Jiang, V. Soghomonian, and J. J. Heremans, Carrier properties of Bi(111) grown on mica and Si(111), Phys. Rev. Mater. **6**, 095003 (2022).

[12] F. Reis, G. Li, L. Dudy, M. Bauernfeind, S. Glass, W. Hanke, R. Thomale, J. Schäfer, and R. Claessen, Bismuthene on a SiC substrate: A candidate for a high-temperature quantum spin Hall material, Science **357**, 287 (2017).

[13] L. Aggarwal, P. Zhu, T. L. Hughes, and V. Madhavan, Evidence for higher order topology in Bi and $Bi_{0.92}Sb_{0.08}$, Nat. Commun. **12**, 4420 (2021).

[14] F. Schindler, Z. Wang, M. G. Vergniory, A. M. Cook, A. Murani, S. Sengupta, A. Yu. Kasumov, R. Deblock, S. Jeon, I. Drozdov, H. Bouchiat, S. Guéron, A. Yazdani, B. A. Bernevig, and T. Neupert, Higher-order topology in bismuth, Nat. Phys. **14**, 918 (2018).

[15] O. Prakash, A. Kumar, A. Thamizhavel, and S. Ramakrishnan, Evidence for bulk superconductivity in pure bismuth single crystals at ambient pressure, Science **355**, 52 (2017).

[16] Y. Hirai, N. Yoshikawa, M. Kawaguchi, M. Hayashi, S. Okumura, T. Oka, and R. Shimano, Anomalous Hall effect of light-driven three-dimensional Dirac electrons in bismuth, arXiv:2301.06072.

[17] F. D. M. Haldane, Model for a quantum Hall effect without Landau levels: Condensed-matter realization of the "parity anomaly," Phys. Rev. Lett. **61**, 2015 (1988).

[18] C.-Z. Chang, J. Zhang, X. Feng, J. Shen, Z. Zhang, M. Guo, K. Li, Y. Ou, P. Wei, L.-L. Wang, Z.-Q. Ji, Y. Feng, S. Ji, X. Chen, J. Jia, X. Dai, Z. Fang, S.-C. Zhang, K. He, Y. Wang *et al.* Experimental observation of the quantum anomalous Hall effect in a magnetic topological insulator, Science **340**, 167 (2013).

[19] M. Serlin, C. L. Tschirhart, H. Polshyn, Y. Zhang, J. Zhu, K. Watanabe, T. Taniguchi, K. Balents, and A. F. Young, Intrinsic quantized anomalous Hall effect in a moiré heterostructure, Science **367**, 900 (2020).

[20] O. Yu, R. Allgayer, S. Godin, J. Lalande, P. Fossati, C. Hsu, T. Szkopek, and G. Gervais, Method of mechanical exfoliation of bismuth with micro-trench structures, J. Appl. Phys. **134**, 244302 (2023).

[21] M. Ozhukil Valappil, A. Ganguly, J. Benson, V. K. Pillai, S. Alwarappan, and P. Papakonstantinou, Bismuthene nanosheets produced by ionic liquid assisted grinding exfoliation and their use for oxygen reduction reaction, RSC Adv. **10**, 43585 (2020).

[22] B. Yang, X. Li, Y. Cheng, S. Duan, B. Zhao, W. Yi, C. Wang, H. Sun, Z. Wang, D. Gu, S. Chen, and X. Liu, Liquid phase exfoliation of bismuth nanosheets for flexible all-solid-state supercapacitors with high energy density, J. Mater. Chem. C **8**, 12314 (2020).

[23] E. I. Rogacheva, S. N. Grigorov, O. N. Nashchekina, S. Lyubchenko, and M. S. Dresselhaus, Quantum-size effects in *n*-type bismuth thin films, Appl. Phys. Lett. **82**, 2628 (2003).

[24] See Supplemental Material at http://link.aps.org/supplemental/10.1103/PhysRevB.109.L121406 for characterization of the 68 nm vdP bismuth device (main text) and AHE signature in 29 nm and 69 nm comb bismuth devices.

[25] C. Rodríguez-Fernández, K. Akius, M. Morais de Lima, Andres Cantarero, J. M. van Ruitenbeek, and C. Sabater, Raman signal reveals the rhombohedral crystallographic structure in ultra-thin layers of bismuth thermally evaporated on amorphous substrate, Mater. Sci. Eng., B **270**, 115240 (2021).

[26] E. S. Walker, S. R. Na, D. Jung, S. D. March, J.-S. Kim, T. Trivedi, W. Li, L. Tao, M. L. Lee, K. M. Liechti, D. Akinwande, and S. R. Bank, Large-area dry transfer of single-crystalline epitaxial bismuth thin films, Nano Lett. **16**, 6931 (2016).

[27] F. D. Hardcastle and I. E. Wachs, The molecular structure of bismuth oxide by Raman spectroscopy, J. Solid State Chem. **97**, 319 (1992).

[28] A. J. Salazar-Pérez, M. A. Camacho-Lopez, R. A. Morales-Luckie, V. Sanchez-Mendieta, F. Urena-Nunez, and J. Arenas-Alatorre, Structural evolution of Bi_2O_3 prepared by thermal

oxidation of bismuth nano-particles, Superficies y Vacío **18** (2005).
[29] J. A. Steele and R. A. Lewis, *In situ* micro-Raman studies of laser-induced bismuth oxidation reveals metastability of β-Bi_2O_3 microislands, Opt. Mater. Express **4**, 2133 (2014).
[30] C. A. Kukkonen and K. F. Sohn, The low-temperature electrical resistivity of bismuth, J. Phys. F: Met. Phys. **7**, L193 (1977).
[31] R. A. Hoffman and D. R. Frankl, Electrical transport properties of thin bismuth films, Phys. Rev. B **3**, 1825 (1971).
[32] D. L. Partin, J. Heremans, D. T. Morelli, C. M. Thrush, C. H. Olk, and T. A. Perry, Growth and characterization of epitaxial bismuth films, Phys. Rev. B **38**, 3818 (1988).
[33] H. H. Sample, W. J. Bruno, S. B. Sample, and E. K. Sichel, Reverse–field reciprocity for conducting specimens in magnetic fields, J. Appl. Phys. **61**, 1079 (1987).
[34] A. L. Jain and S. H. Koenig, Electrons and holes in bismuth, Phys. Rev. **127**, 442 (1962).
[35] A. L. Jain, S. K. Suri, and K. Tanaka, Charge carrier densities and mobilities in bismuth, Phys. Lett. A **28**, 435 (1968).
[36] S. Kochowski and A. Opilski, Concentration and mobility of charge carriers in thin polycrystalline films of bismuth, Thin Solid Films **48**, 345 (1978).
[37] F. Gity, L. Ansari, M. Lanius, P. Schüffelgen, G. Mussler, D. Grützmacher, and J. C. Greer, Reinventing solid state electronics: Harnessing quantum confinement in bismuth thin films, Appl. Phys. Lett. **110**, 093111 (2017).
[38] Y. Zabila, M. Marszalek, M. Krupinski, A. Zarzychi, and M. Perzanowski, Magnetotransport properties of semi-metallic bismuth thin films for flexible sensor applications, Coatings **11**, 175 (2021).
[39] Z. Zhu, B. Fauqué, K. Behnia, and Y. Fuseya, Magnetoresistance and valley degree of freedom in bulk bismuth, J. Phys.: Condens. Matter **30**, 313001 (2018).
[40] Z. Zhu, J. Wang, H. Zuo, B. Fauqué, R. D. McDonald, Y. Fuseya, and K. Behnia, Emptying Dirac valleys in bismuth using high magnetic fields, Nat. Commun. **8**, 15297 (2017).
[41] A. Iwasa, A. Kondo, S. Kawachi, K. Akiba, Y. Nakanishi, M. Yoshizawa, M. Tokunaga, and K. Kindo, Thermodynamic evidence of magnetic-field-induced complete valley polarization in bismuth, Sci. Rep. **9**, 1672 (2019).
[42] L. S. Lerner, Shubnikov-de Haas effect in bismuth, Phys. Rev. **127**, 1480 (1962).
[43] S. Otake, M. Momiuchi, and N. Matsuno, Temperature dependence of the magnetic susceptibility of bismuth, J. Phys. Soc. Jpn. **49**, 1824 (1980).
[44] B. C. Camargo, P. Gierłowski, A. Alaferdov, I. N. Demchenko, M. Sawicki, K. Gas, and Y. Kopelevich, Anomalous Hall effect in bismuth, J. Magn. Magn. Mater. **525**, 167581 (2021).
[45] M.-Y. Yao, F. Zhu, C. Q. Han, D. D. Guan, C. Liu, D. Qian, and J.-F. Jia, Topologically nontrivial bismuth(111) thin films, Sci. Rep. **6**, 21326 (2016).
[46] M.-Y. Liu, Y. Huang, Q.-Y. Chen, Z.-Y. Li, C. Cao, and Y. He, Strain and electric field tunable electronic structure of buckled bismuthene, RSC Adv. **7**, 39546 (2017).
[47] B. Roy and V. Juricic, Unconventional superconductivity in nearly flat bands in twisted bilayer graphene, Phys. Rev. B **99**, 121407(R) (2019).
[48] C.-C. Hsu, M. L. Teague, J.-Q. Wang, and N.-C. Yeh, Nanoscale strain engineering of giant pseudo-magnetic fields, valley polarization, and topological channels in graphene, Sci. Adv. **6**, eaat9488 (2020).
[49] Donovan and G. T. Conn, LXIX. The electrical conductivity of bismuth fibres: II. Anomalies in the magneto-resistance, London Edinburgh Mag. J. Sci. **41**, 770 (1950).
[50] G. T. Conn and B. Donovan, Anomalous magneto-resistance effects in bismuth, Nature (London) **162**, 336 (1948).